A survey of the polar cap density based on Cluster EFW probe measurements: Solar wind and solar irradiation dependence

S. Haaland,[1,2] K. Svenes,[3] B. Lybekk,[4] and A. Pedersen[4]

Received 10 October 2011; revised 16 November 2011; accepted 22 November 2011; published 31 January 2012.

[1] The plasma density above the Earth's polar caps provide crucial information about the state of the magnetosphere. This region of space is known for its tenuous plasma and extremely low plasma densities, thus making traditional measurements with particle and plasma instruments extremely difficult. A new method based on spacecraft potential measurements from the electric field instrument onboard the Cluster satellites has shown that more reliable density measurements can be obtained. In this paper, we utilize this method and present a survey of the polar cap densities and the response to changes in the solar irradiation, solar wind parameters as well as processes internal to the magnetosphere. Our observations spans a time interval of almost 10 years, thus covering almost a full solar cycle. The observations seem to confirm that solar irradiance, and thus ionization through UV absorption in the atmosphere is the most important mechanism controlling the polar cap cold plasma density. We also find positive correlations between polar cap density and solar wind density and solar wind dynamic pressure, as well as geomagnetic activity levels.

Citation: Haaland, S., K. Svenes, B. Lybekk, and A. Pedersen (2012), A survey of the polar cap density based on Cluster EFW probe measurements: Solar wind and solar irradiation dependence, *J. Geophys. Res.*, *117*, A01216, doi:10.1029/2011JA017250.

1. Introduction

[2] The plasma density above the Earth's polar caps provide crucial information about the magnetosphere - ionosphere coupling. On one side, the ionosphere is strongly influenced by solar activity, in particular irradiance in the extreme ultraviolet range (EUV) which modulates the ionization rate. On the other hand, space weather effects like solar flares, coronal mass ejections and subsequent compression of the magnetosphere can cause sudden density changes. The former primarily affects the density in low altitudes on the dayside whereas density variations due to space weather effects can be observed at all altitudes.

[3] Since the ionosphere and magnetosphere are magnetically connected, plasma outflow can propagate changes in the lower ionosphere to higher altitudes [*André and Yau*, 1997; *Hultqvist et al.*, 1999]. The outflow of plasma from the ionosphere mainly occurs at high latitudes [*Chappell*, 1988; *Moore et al.*, 1997] and can thus affect the density (and composition) in the magnetically connected polar cap and lobe regions. Transport of cold plasma from the ionosphere to the magnetosphere is slow, so effects of enhanced solar irradiance are not observed immediately in the high altitude polar caps.

[4] The polar cap regions also play an important role in the large scale plasma circulation initiated when solar wind magnetic field connects with the Earth's magnetic field on the dayside magnetopause [*Dungey*, 1961]. Magnetic field lines, and plasma of magnetosheath origin attached to the field, are convected across the polar caps via the tail lobes to the nightside magnetotail. Enhanced dayside reconnection will therefore lead to increased transport of plasma across the polar caps. There is also some evidence for plasma entry via the cusp [see, e.g., *Hultqvist et al.*, 1999, and references therein]. The solar wind and magnetosheath are therefore also sources of plasma in the polar cap region.

[5] The low particle density above the high altitude polar cap regions of the magnetosphere makes direct measurements with plasma instruments difficult. In addition to the low count rates, measurements are often severely affected by spacecraft charging. Sunlit surfaces of a spacecraft will emit photo electrons. In a tenuous plasma, providing a small return current, the spacecraft will therefore eventually be charged to large positive potentials. As a result, a significant part of the low energy ion population will be shielded from the detectors, and moment calculations will not be reliable. An additional challenge is that the low density encountered in this region requires either long integration times or large geometric factors of the sensor to obtain sufficient number of counts for reliable moment calculations.

[6] For this reason, studies of cold plasma density in the high altitude polar cap region using particle instruments are

[1]Max-Planck-Institute for Solar System Research, Katlenburg-Lindau, Germany.
[2]Department of Physics and Technology, University of Bergen, Bergen, Norway.
[3]Norwegian Defence Research Establishment, Kjeller, Norway.
[4]Department of Physics, University of Oslo, Oslo, Norway.

0148-0227/12/2011JA017250

rare. A notable exception is the study by *Su et al.* [1998]. They used ion moments from the Thermal Ion Dynamics Experiment (TIDE) onboard the Polar spacecraft during a limited time period between April and May 1996 when the on board Plasma Source Instrument (PSI) [see *Moore et al.*, 1995, 1997] was operating and stabilized the spacecraft potential to around 2 V.

[7] Active and passive sounders, such as e.g., WDB (Wide-Band Plasma Wave Investigation) [see *Gurnett et al.*, 1997] or WHISPER (Waves of HIgh frequency and Sounder for Probing of Electron density by Relaxation) [see *Trotignon et al.*, 2001], which rely on the identification of a plasma resonance line or a cut-off frequency in the wave spectrum, can provide very accurate measurements of electron densities. However, even this technique has some limitations in this region; It is not always possible to automatically determine a unique resonance line in the spectrum, and the analysis can therefore sometimes require time consuming, manual inspection of the data. In active sounding mode, the Cluster WHISPER experiment involves excitation of the plasma by sweeping over a frequency range. The lowest excitation frequency is approximately 4 kHz. This corresponds to a lower limit of approximately 0.2 cm^{-3} for density measurements. Even with a reliable identification of a resonance or cut-off frequency, results from plasma wave instruments can be skewed by the presence of photoelectrons from the spacecraft surface, or mismatch between the observed cut-off frequency and the local plasma density [*Ishisaka et al.*, 2001].

[8] Due to these limitations, most of our recent knowledge about the density in the high altitude polar cap and lobe regions has therefore been based on measurements from double probe instruments [e.g., *Escoubet et al.*, 1997; *Pedersen et al.*, 1998, 2001; *Laakso et al.*, 2002; *Pedersen et al.*, 2008; *Engwall et al.*, 2006, 2009a, and references therein].

[9] In a recent paper, *Lybekk et al.* [2012] revisited the spacecraft potential technique and used calibrated Cluster data combined with measurements of solar irradiance to calculate more accurate cold plasma density values for the complete Cluster period 2001–2010. In this paper, we present a survey of polar cap density obtained with this technique during almost 10 years of EFW (Electric Field and Wave Experiment) [see *Gustafsson et al.*, 2001] operation. This study is a follow-up on the paper by *Lybekk et al.* [2012], where the background theory and calibration of the double probe technique was explained.

[10] This paper is organized as follows: In section 2, we give a description of the method and data set used for the survey, as well as an overview of auxiliary data used to establish solar wind conditions and the geomagnetic activity level. In section 3 we discuss correlations and try to identify source regions and discuss correlations between the density and external drivers such as solar wind and solar irradiance. Finally, section 4 summarizes the main results of the paper.

2. Methodology and Data

2.1. EFW Based Density Estimation

[11] As demonstrated by *Pedersen et al.* [2008], a functional relationships between the spacecraft potential, V_{sp}, and the ambient electron density, N_e, can be established:

$$N_e(EFW) = Ae^{-V_{sp}/B} + Ce^{-V_{sp}/D}\left[\mathrm{cm}^{-3}\right] \quad (1)$$

[12] On Cluster, the spacecraft potential, V_{sp}, is obtained routinely from the EFW double probe experiment. This relation only holds if there are no artificial potential controls, such as the active Spacecraft Control (ASPOC) ion emitters [*Riedler et al.*, 1997; *Torkar et al.*, 2001] in operation, and also no significant electron currents from the Electron Drift Instrument (EDI) [see *Paschmann et al.*, 1997, 2001]. Also, the method has been calibrated for densities up to approximately 1 cm^{-3}, spacecraft voltages up to ≈60 V, and thus electron energies up to 60 eV.

[13] The coefficients A, B, C and D are not constants, but changes over the years due to changes in UV radiation and possibly changes in the conducting surface of the spacecraft. However, by a thorough inter calibration between EFW and the Cluster Plasma Electron And Current Experiment (PEACE) [see *Johnstone et al.*, 1997], WHISPER and WDB instruments, in regions where these provide reliable measurements, the value of the coefficients can be established for that epoch. It has thus been possible to estimate the density of low energy electrons for the whole Cluster period 2001–2010, and simplified the above expression so that only the coefficients A and B have to be determined for each epoch and spacecraft [*Lybekk et al.*, 2012].

[14] In the polar cap region (and most of the magnetosphere), the total concentration of positive and negative charges within a volume is approximately equal (electrostatic forces will immediately redistribute any large scale charge imbalance). The above expression for electron density is therefore also a proxy for ion density, and we will hereafter simply use the term cold (due to the 0–60 eV energy range) plasma density or simply density.

2.2. Accuracy of Density Estimates

[15] Since the uncertainty in an individual Ne estimate depends on several factors, it is difficult to provide a single error estimate for the method.

[16] First, V_{sp} in equation (1) is the measured voltage difference between the spacecraft body and the EFW probes. Ideally, the probes should have the same potential as the ambient, undisturbed plasma. In practice, however, this is not possible, and *Pedersen et al.* [2008] has estimated that the probe potential is about 2 ± 0.5 V. This error is thus less critical for high spacecraft potentials (corresponding to low densities), but will play a role for the accuracy in regions with lower spacecraft potentials (higher densities).

[17] The coefficients A and B in equation (1) primarily depend on the mean electron energy and EUV radiation, and are determined from cross calibration with the PEACE, CIS, WHISPER and WDB instruments in regions where one or more of these instruments provide reliable measurements. Spread in these parameters will therefore give an additional uncertainty in the N_e determination.

[18] Most of the measurements used in this paper (see Figure 1) are obtained in the polar cap region where the mean electron energy is fairly low, and the spacecraft potential is in the range 30–40 V. For this range, *Lybekk*

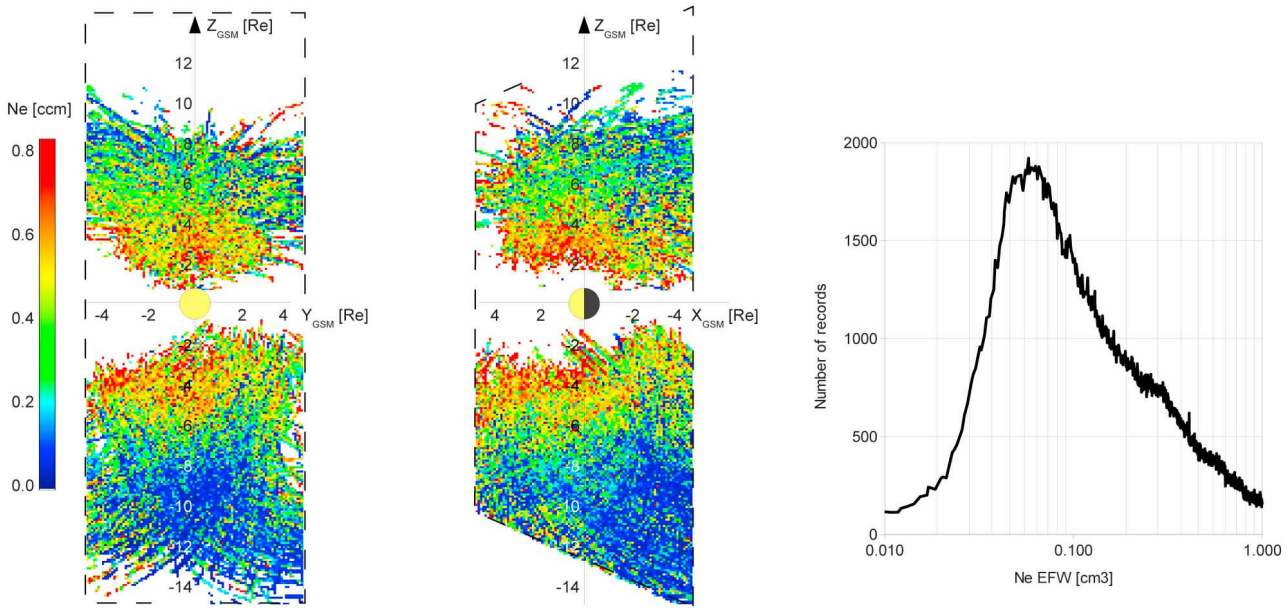

Figure 1. (left) YZ_{GSM} projection of the two 10 × 20 × 15 R_E data volumes in northern and southern hemisphere, respectively. Cluster orbits with the densities as color codes are shown. (middle) Ditto XZ projection. The coverage is fairly good, and some regions, e.g., the lobes (blue color - low density) are apparent from these plots. (right) Density distribution for the full data set. Due to the skewness of the distribution, the moments; mean, median and mode, are different.

et al. [2012] estimate that the uncertainty in N_e is approximately ±20%.

[19] For more detailed information about the generation, calibration and validation of the EFW density measurements, we refer to *Lybekk et al.* [2012].

2.3. Data Set Characteristics

[20] The full EFW data set is based on density measurements obtained from Cluster from two regions within 10 × 20 × 15 R_E (X_{GSM} × Y_{GSM} × Z_{GSM}) boxes in the northern and southern hemisphere, respectively. These limits may seem somewhat arbitrary, but was chosen to exclude measurements from the magnetopause/magnesheath region and the plasma sheet, where the method is less accurate due to a hotter plasma. Two different projections of these boxes and the individual orbits with color coded density values are illustrated in Figure 1 (left). The data coverage is fairly good, and some regions, e.g., the lobes (blue color - low density) are apparent from this plot. For a survey of cold plasma density in the nightside magnetotail lobes at larger distances, we refer to the paper by *Svenes et al.* [2008].

[21] The full data set consist of 538′644 one minute averages (≃9000 hours) of the electron density, primarily based on measurements from Cluster C4 where EDI is not operating and C2 where EDI was operating until early 2004 only. There is also a substantial number of records from the other two spacecraft obtained when EDI was turned off or operating with low beam currents so that reliable density measurements could be inferred. Each data record also contains the spacecraft position, solar wind parameters and geomagnetic activity indices used for mapping as well as information about solar irradiance used to study dependencies.

[22] We only use data where reliable density values could be calculated, and we also discarded records with data gaps or fill values in any of the ancillary data. To avoid remaining contamination from magnetosheath and the plasma sheet, we also removed records where the omnidirectional ≃20 keV electron flux from the Cluster RAPID (Research with Adaptive Particle Imaging Detectors) [see *Wilken et al.*, 1997] instrument was above 1000 cm^{-2} s^{-1} sr^{-1}. Due to the evolution of the spacecraft orbit, with the line of apsides tilting further down with time, the coverage is better for southern hemisphere than for the northern hemisphere. We will not focus on seasonal dependencies or north-south asymmetries, so all values and correlations are based on data combined from both hemispheres. As pointed out by, e.g., *Laakso et al.* [2002] and *Kitamura et al.* [2011], solar zenith angle variations and hence seasonal variations are primarily affecting lower altitudes, and are not believed to play any role at the altitudes discussed in this paper.

[23] Figure 1 (right) shows the distribution of density values in the data set. The full distribution is highly non-gaussian, with a mean, median and mode of 0.326, 0.255 and 0.057 cm^{-3}, respectively, and a standard deviation of 0.254 cm^{-3} (the mode is calculated as the density value with highest frequency within a 1000 bin distribution). When dividing the data into subsets according to driver parameters (see section 3), we sometimes obtain distributions with a flatter peak or several peaks (bimodal, multimodal or partly uniform distributions). In such cases the mode moment is not unique. We will therefore use the median density value when discussing correlation and dependencies in the next sections.

[24] Figure 2 provides further information about the spatial distribution of the measurements. To avoid inclusion of

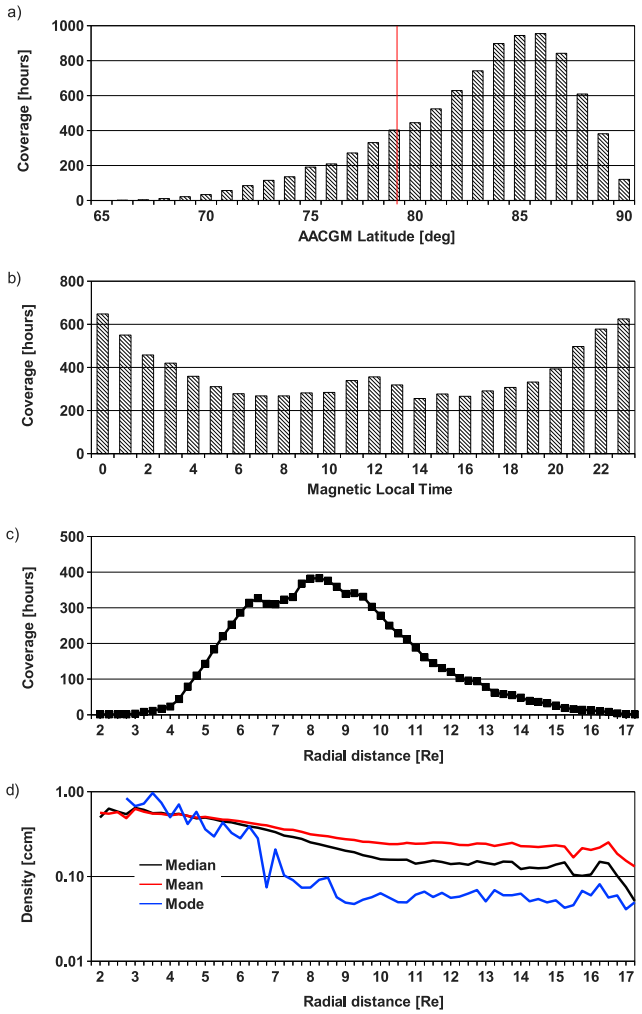

Figure 2. Data set characteristics for the full data set. (a) Data coverage as function of corrected geomagnetic latitude. Most of the measurements are obtained a latitudes above 80° CGM latitude (indicated by vertical red line). (b) Coverage versus local time sector. Due to the orbit of Cluster, there is a better coverage in the midnight and noon sectors. (c) Coverage versus radial distance. The majority of the observations are taken between 6–10 R_E radial distance. (d) The three density moments (mean, median, mode) as function of radial distance. For radial distances below 3 R_E, the mode is undefined.

data from e.g., the auroral zone, we only use data with magnetic foot points poleward of 80° corrected geomagnetic (CGM) [see, e.g., *Gustafsson et al.*, 1992] latitude for the correlation analysis discussed in the next section. This constraint is probably very conservative, but as seen from Figure 2a the majority (≈400′000 records = 70% of total data set) of the measurements are obtained at high latitudes anyway, so discarding measurements with magnetic foot points further equatorward does not severely reduce the amount of data. The local time distribution of the measurements is primarily a result of the orbit of Cluster, with better coverage in the midnight sector than in the morning and evening sectors. As seen in Figure 2c, most of the measurements are obtained in the 6–10 R_E altitude range. With the exception of the Polar results by *Su et al.* [1998] and *Laakso et al.* [2002], few systematic studies of density variations exist for this altitude range. Figure 2d shows the density as function of radial distance. For radial distances above 4 R_E, both the median and mean density show a smooth decline in density toward higher altitude. The mode shows a distinct change between ≃6–7 R_E altitude (the mode moment is well defined in this region). That is, below ≃6 R_E, the typical (most frequent) values of the density are significantly higher than those beyond ≃7 R_E. This distinct demarcation may be an signature of two different sources; the values inside 6 R_E may be related to ionospheric outflow, whereas the lower values at higher altitudes may reflect the much lower background plasma density of solar wind origin.

[25] The obtained densities are comparable to those reported by *Su et al.* [1998]. From a limited number of Polar apogee passes above the northern polar cap (approximately 8 R_E altitude), they found an average proton density of approximately 0.3 cm^{-3}. During perigee (approx. 5000 km altitude) passes, spacecraft charging is less of an issue, and *Su et al.* [1998] employed an iterative scheme to fill in the missing portion of the distribution shielded by the residual spacecraft potential, before calculating the moments. In those altitudes, the Polar results revealed a dramatic change (more than one order of magnitude) in density in the transition region between the sunlit and dark ionosphere, consistent with solar illumination control of the ionization.

[26] *Laakso et al.* [2002] also used Polar observation, but based their measurements on the Electric Field Instrument (EFI) [see *Harvey et al.*, 1995] and a technique similar our. They reported average densities in the range 0.03 – 0.3 cm^{-3} for 5–9 R_E altitudes, and also found a factor 2–5 higher densities between low and high Kp values. *Laakso et al.* [2002] also noted strong seasonal density variations during perigee passes, suggesting solar illumination modulation of the density.

2.4. Solar Wind and Auxiliary Data

[27] Information about solar wind velocity, density, pressure and the interplanetary magnetic field (IMF) were obtained from the OMNI data set available from CDAWEB. These data are collected from various spacecraft in the solar wind and time shifted to be representative for the conditions at the upstream magnetopause [*King and Papitashvili*, 2005; *Weimer and King*, 2008]. The OMNI data set also contains the KP, Dst and AE indices used to classify the geomagnetic disturbance level of the magnetosphere.

[28] Accurate measurements of solar irradiance is important for the calibration of the method (see details in work by *Lybekk et al.* [2012]). For this study, we have used two different measures of solar irradiance. The F10.7 index is a measure of the noise generated by the sun at a wavelength of 10.7 cm. Daily values of this index are measured at local noon at the Penticton Radio Observatory in Canada. Historically, this index has been used as a proxy for the solar output responsible for photo ionization in the Earth's ionosphere. The F10.7 index is available for the full period

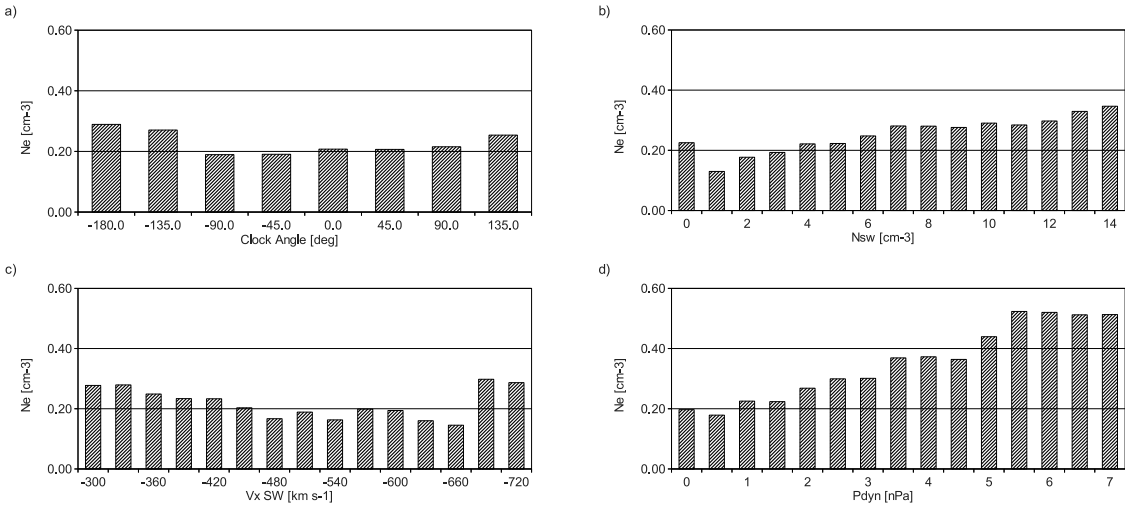

Figure 3. Polar cap density as function of (a) 8 different IMF clock angle sectors, (b) solar wind density, (c) solar wind velocity, and (d) solar wind dynamic pressure. In Figure 3a, a clock angle of 0° corresponds to northward IMF; ±180° corresponds southward IMF. The horizontal axis labels in Figures 3b–3d indicate the lower limit of the parameter range (e.g., in Figure 3d, the label 0 means a dynamic pressure from 0–0.5 nPa).

2001–2010 covered by this study. A second, more direct set of observations is provided by the Thermosphere, Ionosphere, and Mesosphere Energetics and Dynamic (TIMED) spacecraft. We here utilize the EUV irradiance in the 0–105 nm range, which corresponds to photon energies above 12 eV. TIMED flies in a 625 km altitude, 74° inclination circular orbit, and the EUV measurements are based on at least 3 min of observations for each orbit [*Woods et al.*, 2005]. Measurements from TIMED are available from 2002 and onwards.

[29] The combination of carefully calibrated Cluster measurements of cold plasma density with properly shifted solar wind data and direct measurements of the solar irradiation makes the *Lybekk et al.* [2012] data set the most accurate and extensive (both in terms of spatial coverage and time span) collection of polar cap density measurements available today.

3. Correlations Between Polar Cap Density and External Drivers

[30] As seen in Figure 1, the mean, median and mode for the full data set was 0.326, 0.255, and 0.057 cm^{-3} respectively. If we only include data above 80° CGM latitude, i.e., only measurements taken along magnetic field lines with their foot point in the polar cap, the corresponding numbers are 0.301, 0.225 and 0.059 cm^{-3}, respectively, with a standard deviation of 0.245 cm^{-3}.

[31] In order to find out what controls the density, we created a number of subsets containing only data from records where driver parameters (disturbance level, solar wind, solar irradiance) were within certain ranges. As a measure of spread in each subset, we also calculated the standard deviation. Standard deviations of these subsets are not shown in the plots, but are typically similar or slightly smaller than the average density value itself. The correlation between the driver parameters and the density will provide information about factors controlling the density. Below, we discuss some of these dependencies in detail.

3.1. IMF Influence

[32] Figure 3 demonstrates how the median density varies with solar wind and IMF variations. To better demonstrate the relative importance of the various drivers, we use the same scale in all plots. Figure 3a shows the median density binned into 8 different IMF sectors. To construct this plot, we simply take the prevailing IMF orientation (within ±22.5° of the given value) without requiring that the IMF should remain stable in that direction for any amount of time. Nevertheless, the plot gives a good impression of the role of IMF orientation for the polar cap electron density.

[33] During southward IMF, the density is approximately 15% higher than the median value of the entire data set. Conversely, a northward directed IMF is associated with an approximately 25% lower density. There appears to be a slightly higher median density for positive IMF By dominated conditions than for negative IMF By, but the significance of this asymmetry is not clear. We also tried to divide this data set into two altitude ranges; below 6 R_E and above 7 R_E (see discussion concerning Figure 2), but did not find any significant difference in IMF response for the two altitude ranges.

[34] There are two conceivable explanations for the IMF dependency; Enhanced solar wind entry on the dayside or enhanced ionospheric outflow. However, the former is less likely, as magnetosheath plasma typically have higher energies and is hotter [*Sandholt et al.*, 1999; *Øieroset et al.*, 2008]. Enhanced ion outflow, on the other hand, is largely governed by geomagnetic activity [e.g., *André and Yau*, 1997; *Yau and Andre*, 1997; *Moore and Horwitz*, 2007]. Geomagnetic activity again, is primarily modulated by the IMF and dayside reconnection [*Burton et al.*, 1975].

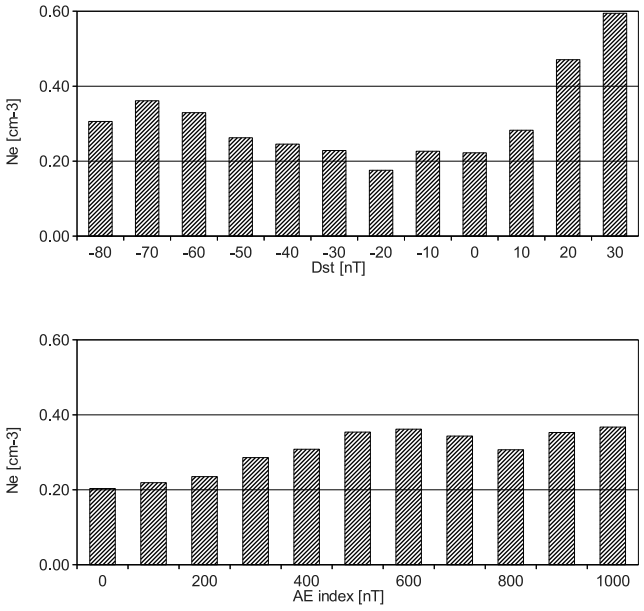

Figure 4. Correlation between polar cap density and geomagnetic activity level. (top) Polar cap density as function of the Dst index. (bottom) Density as function of AE index. In general, high geomagnetic activity is associated with higher density. Large density values for positive Dst is probably due to compression of the whole magnetosphere.

3.2. Solar Wind Dependencies

[35] Figures 3b–3d show correlation to the other key parameters of the solar wind. Both solar wind density (Figure 3b) and solar wind bulk velocity (Figure 3c) as well as the derived solar wind dynamic pressure ($p_{sw} \propto n_{sw}V_{sw}^2$ - shown in Figure 3d) are intrinsically unrelated to the IMF orientation. The positive correlation with dynamic pressure can probably be explained by compression effects; A high ram pressure will compress the entire magnetosphere. The correlation with solar wind density can partly be related to the same effect, but may also be due to enhanced transfer of solar wind plasma by some mechanism (e.g., under southward IMF conditions). Since both the dynamic pressure and the solar wind density are correlated with geomagnetic activity [*Burton et al.*, 1975; *Förster et al.*, 2008] and disturbance level, other effects such as enhanced ionospheric outflow probably also play a role.

[36] For solar wind velocities up to about 700 km s^{-1}, there seems to be an anti correlation between the solar wind velocity and polar cap density. Several effects probably play a role here. First, the slow solar wind typically have a higher density than the fast solar wind [e.g., *McComas et al.*, 1998; *Feldman et al.*, 2005]. The resulting ram pressure ($p_{sw} \propto n_{sw}V_{sw}^2$), and thus the compression of the magnetosphere is roughly constant. This is also apparent from the OMNI data set used; there is an anticorrelation between solar wind speed and density, and thus little or no correlation between solar wind speed and ram pressure.

[37] The high polar cap densities for solar wind velocities above $\simeq$700 km s^{-1}, are related to single events (there are only about 50 hours of observations with solar wind velocities above 700 km s^{-1}) such as coronal mass ejections (CMEs).

3.3. Disturbance Level

[38] In Figure 4, we plot the density as function of the Dst and AE indices. The Dst index, mainly reflects large scale geomagnetic storm timescales (typically several days from initial phase to recovery). The AE index, on the other hand, primarily reflects short-lived (minutes to hours) and localized processes, such as substorms and bursty bulk flow events in the plasma sheet. These processes are coupled to the nightside auroral zone through field aligned currents, and typically combined with auroral activity.

[39] Unlike the Polar results by *Su et al.* [1998], obtained in the high altitude polar cap region, we find a correlation between magnetic activity and density: If we ignore positive Dst values, the density varies more than a factor 2 between storm activity (large negative Dst values) and more quiet conditions. Also apparent is a strong compression effect for positive Dst. The correlation between density and the AE index shows a similar behavior. Up to AE values of $\simeq$700 nT, there is a clear positive correlation, although the difference in density between the lowest and highest auroral activity level is less than a factor 2. The general tendency, with higher densities during disturbed conditions and less during quiet periods is also apparent if we organize the data according to the Kp index.

[40] Except from the compression response for positive Dst values, the disturbance level dependency is probably a reflection of the enhanced ion outflow from the polar ionosphere. It has been suggested that the outflow becomes more effective as a result of larger ambipolar electric field in the ionosphere and thus a more efficient acceleration up from the ionosphere, in particular from the cusp/cleft area [*Lockwood et al.*, 1985a, 1985b; *Moore and Horwitz*, 2007; *Young et al.*, 1982].

3.4. Solar Irradiance

[41] Finally, Figure 5 shows the correlation between solar irradiance and cold plasma density. We plot the density versus both the F10.7 index and the EUV measurements from the TIMED spacecraft. Note that the latter correlation is based on values after 2002 only. Except from a few bins,

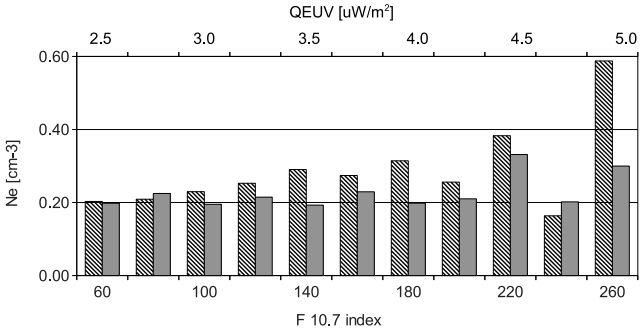

Figure 5. Polar cap density as function of solar irradiance. Hatched bars and lower horizontal axis show correlation with the F10.7 index, solid gray bars and upper horizontal axis show correlation with TIMED extreme ultraviolet (EUV - wavelengths between 0 and 105 nm) measurements.

the results show a positive correlation between polar cap density and solar radiation, when using the daily F10.7 index.

[42] The correlation with the measured EUV from TIMED is more variable, but high EUV values (the 4.5 and 5.0 μWm^{-2} bins) show a much higher density values than for periods with less EUV intensity. Keep in mind that the TIMED EUV measurements have an approximately 97 minute cadence (once per orbit). This timescale is probably comparable or smaller than the transport time from the ionosphere (where the EUV ionization takes place) to Cluster altitudes. This may explain the low correlation between high altitude cold plasma density and the direct EUV measurements.

[43] Since irradiance is largely independent from other driver parameters these results seem to confirm the claim that enhanced ionization in the ionosphere is the most important source for plasma in the polar cap and lobe area [*Chappell et al.*, 1987]. The results are also consistent with the *Su et al.* [1998] findings based on Polar observations.

3.5. Source of Plasma

[44] As discussed above, there are essentially two conceivable sources for the plasma population in the high altitude polar cap region; outflow from the terrestrial ionosphere, or solar wind entry, either direct as a result of reconnection or possible via other diffusive effects along the magnetopause [*Hultqvist et al.*, 1999].

[45] Our results show that there is a clear connection between solar irradiance and polar cap plasma density; higher irradiance leads to higher plasma density. This is an indicator of an ionospheric source, and supports the idea that outflow from the ionosphere is a significant contributor to the plasma in the magnetosphere. The mechanisms, essentially increased photoionization due to UV radiation, are also well established. Earlier studies [e.g., *Chappell et al.*, 1987; *Engwall et al.*, 2009b] estimate that the ion outflow rate is of the order 10^{26} s^{-1}.

[46] We also find positive correlations between other solar wind parameters. Response to the solar wind ram pressure is probably a consequence of compression of the whole magnetosphere, and does not necessarily indicate an enhanced entry of plasma from the solar wind. Higher polar cap densities are also observed during periods with southward IMF. This could indicate a entry of magnetosheath plasma. Several mechanisms for plasma transfer exist (see, e.g., *Paschmann* [1997] for an overview), but the observed correlations could also be a result of secondary effects; A southward IMF is often associated with geomagnetic activity (storms, substorms) which will have an impact on ionospheric outflow. *Paschmann* [1997] estimated that the rate of entry of solar wind plasma across the whole dayside magnetopause is on the order of 10^{26} s^{-1}, i.e., comparable to the ion outflow rate. The entry is primarily attributed to dayside reconnection, whereas transfer due to other processes such as diffusion, impulsive plasma penetration [*Lemaire and Roth*, 1978] are many orders of magnitude smaller.

[47] During extended periods of northward IMF conditions, a cold dense plasma sheet is often observed [e.g., *Fujimoto et al.*, 2002]. Simulations and comparisons to Cluster data [*Øieroset et al.*, 2005; *Li et al.*, 2005] suggest that this population is formed by high latitude (i.e., poleward of cusp) reconnection which captures magnetosheet plasma which is subsequently cooled [*Wing et al.*, 2006] and slowly convected to the tail plasma sheet. Our measurements at high altitudes may thus include the coldest part of this slowly convecting, cold population.

[48] Recall that the technique used to establish the electron density is limited to energies around a few eV up to approximately 60 eV (limited by spacecraft potential). Since outflowing plasma are exposed centrifugal acceleration [*Nilsson et al.*, 2008, 2010], the method may underestimate the density at higher altitudes, where the plasma has been accelerated to energies outside the detection range.

4. Summary

[49] We have used 10 years of electron density measurements derived from the Cluster EFW probe potential to study cold plasma density variations in the 2–17 R_E altitude region above the polar caps. The data set by *Lybekk et al.* [2012] probably contains the most comprehensive and accurate measurements of cold plasma density for the polar cap regions available today. The full data set is characterized by a fairly large spread in density values, ranging from 0.002 up to 1 cm^{-3} (where 1 cm^{-3} represents the upper limit of the method), with the highest values at low altitudes.

[50] The main findings can be summarized as follows.

[51] 1. For the full data set, the statistical mean, median and mode densities are 0.326, 0.255 and 0.057 cm^{-3}, respectively, with a standard deviation of 0.254 cm^{-3}.

[52] 2. The polar cap plasma density varies with solar activity; This can be explained by UV irradiance, which leads to increased ionization and thus higher electron density. Since the ionosphere and magnetosphere are magnetically linked, changes in ionospheric density at low altitudes are propagated to higher altitudes.

[53] 3. Increased solar wind dynamic pressure (which may be due to either increased solar wind density or velocity) leads to a higher polar cap density. Most of this effect can probably be explained by a compression of the whole magnetosphere.

[54] 4. We also find a correlation between IMF and the density; Southward IMF is associated with higher densities, but it is unclear to what degree this correlation is due to solar wind penetration or secondary effects that enhance ionospheric outflow.

[55] 5. Internal processes in the magnetosphere, such as substorms and bursty bulk flow events (reflected in the AE index) seem to be reflected in the polar cap density; Higher disturbance levels are associated with higher plasma densities. During storms (strong negative Dst), the polar cap density is on average higher then during quiet conditions. Once again, some of this may be explained by increased solar wind plasma entry, but secondary effects as mentioned above also probably play a role.

[56] 6. The cold plasma density in the high altitude polar cap region seems to react slower to fast changes in geomagnetic activity and ionization than at lower altitudes. This can probably be explained by the transport time from the ionosphere where the production takes place to the magnetosphere where our measurements are taken.

[57] **Acknowledgments.** All Cluster data used in this paper have been obtained from the Cluster Active Archive (CAA - see http://caa.estec.esa.int/caa/home.xml). Solar wind data were obtained from the Coordinated Data Analysis Web (CDAWeb - see http://cdaweb.gsfc.nasa.gov/about.html). Computer code used for the calculations in this paper has been made available as part of the QSAS science analysis system. QSAS is provided by the United Kingdom Cluster Science Centre (Imperial College London and Queen Mary, University of London) supported by the United Kingdom Science and Technology Facilities Council (STFC). We also thank the International Space Science Institute, Bern, Switzerland for providing computer resources and infrastructure for data exchange.

[58] Masaki Fujimoto thanks the reviewers for their assistance in evaluating this paper.

References

André, M., and A. Yau (1997), Theories and observations of ion energization and outflow in the high latitude magnetosphere, *Space Sci. Rev.*, *80*, 27–48.

Burton, R. K., R. L. McPherron, and C. T. Russell (1975), An empirical relationship between interplanetary conditions and Dst, *J. Geophys. Res.*, *80*, 4204–4214.

Chappell, C. R. (1988), The terrestrial plasma source—A new perspective in solar-terrestrial processes from Dynamics Explorer, *Rev. Geophys.*, *26*, 229–248.

Chappell, C. R., T. E. Moore, and J. H. Waite Jr. (1987), The ionosphere as a fully adequate source of plasma for the Earth's magnetosphere, *J. Geophys. Res.*, *92*, 5896–5910.

Dungey, J. R. (1961), Interplanetary magnetic field and the auroral zones, *Phys. Rev. Lett.*, *6*, 47–48.

Engwall, E., A. I. Eriksson, M. André, I. Dandouras, G. Paschmann, J. Quinn, and K. Torkar (2006), Low-energy (order 10 eV) ion flow in the magnetotail lobes inferred from spacecraft wake observations, *Geophys. Res. Lett.*, *33*, L06110, doi:10.1029/2005GL025179.

Engwall, E., A. I. Eriksson, C. M. Cully, M. André, P. A. Puhl-Quinn, H. Vaith, and R. Torbert (2009a), Survey of cold ionospheric outflows in the magnetotail, *Ann. Geophys.*, *27*, 3185–3201.

Engwall, E., A. I. Eriksson, C. M. Cully, M. André, R. Torbert, and H. Vaith (2009b), Earth's ionospheric outflow dominated by hidden cold plasma, *Nat. Geosci.*, *2*, 24–27.

Escoubet, C. P., A. Pedersen, R. Schmidt, and P. A. Lindqvist (1997), Density in the magnetosphere inferred from ISEE 1 spacecraft potential, *J. Geophys. Res.*, *102*, 17,595–17,610.

Feldman, U., E. Landi, and N. A. Schwadron (2005), On the sources of fast and slow solar wind, *J. Geophys. Res.*, *110*, A07109, doi:10.1029/2004JA010918.

Förster, S. E., M. Haaland, G. Paschmann, J. M. Quinn, R. B. Torbert, H. Vaith, and C. A. Kletzing (2008), High-latitude plasma convection during northward IMF as derived from in-situ magnetospheric Cluster EDI measurements, *Ann. Geophys.*, *26*, 2685–2700.

Fujimoto, M., T. Mukai, and S. Kokubun (2002), Cold-dense plasma sheet and hot-dense ions in the inner-magnetosphere, *Adv. Space Res.*, *30*, 2279–2288.

Gurnett, D. A., R. L. Huff, and D. L. Kirchner (1997), The wide-band plasma wave investigation, *Space Sci. Rev.*, *79*, 195–208.

Gustafsson, G., N. E. Papitashvili, and V. O. Papitashvili (1992), A revised corrected geomagnetic coordinate system for epochs 1985 and 1990, *J. Atmos. Terr. Phys.*, *54*, 1609–1631.

Gustafsson, G., et al. (2001), First results of electric field and density measurements by Cluster EFW based on initial months of operation, *Ann. Geophys.*, *19*, 1219–1240.

Harvey, P., et al. (1995), The electric field instrument on the Polar satellite, *Space Sci. Rev.*, *71*, 583–596.

Hultqvist, B., M. Øieroset, G. Paschmann, and R. Treumann (1999), Magnetospheric plasma sources and losses: Final report of the ISSI study project on source and loss processes of magnetospheric plasma, *Space Sci. Rev.*, *88*, 1–483.

Ishisaka, K., T. Okada, K. Tsuruda, H. Hayakawa, T. Mukai, and H. Matsumoto (2001), Relationship between the Geotail spacecraft potential and the magnetospheric electron number density including the distant tail regions, *J. Geophys. Res.*, *106*, 6309–6320.

Johnstone, A. D., et al. (1997), Peace: A plasma electron and current experiment, *Space Sci. Rev.*, *79*, 351–398.

King, J. H., and N. E. Papitashvili (2005), Solar wind spatial scales in and comparisons of hourly Wind and ACE plasma and magnetic field data, *J. Geophys. Res.*, *110*, A02104, doi:10.1029/2004JA010649.

Kitamura, N., Y. Ogawa, Y. Nishimura, N. Terada, T. Ono, A. Shinbori, A. Kumamoto, V. Truhlik, and J. Smilauer (2011), Solar zenith angle dependence of plasma density and temperature in the polar cap ionosphere and low-altitude magnetosphere during geomagnetically quiet periods at solar maximum, *J. Geophys. Res.*, *116*, A08227, doi:10.1029/2011JA016631.

Laakso, H., R. Pfaff, and P. Janhunen (2002), Polar observations of electron density distribution in the Earth's magnetosphere. 1. Statistical results, *Ann. Geophys.*, *20*, 1711–1724.

Lemaire, J., and M. Roth (1978), Penetration of solar wind plasma elements into the magnetosphere, *J. Atmos. Terr. Phys.*, *40*, 331–335.

Li, W., J. Raeder, J. Dorelli, M. Øieroset, and T. D. Phan (2005), Plasma sheet formation during long period of northward IMF, *Geophys. Res. Lett.*, *32*, L12S08, doi:10.1029/2004GL021524.

Lockwood, M., J. H. Waite Jr., T. E. Moore, C. R. Chappell, and M. O. Chandler (1985a), The cleft ion fountain, *J. Geophys. Res.*, *90*, 9736–9748.

Lockwood, M., J. H. Waite Jr., T. E. Moore, C. R. Chappell, and J. F. E. Johnson (1985b), A new source of suprathermal O(+) ions near the dayside polar cap boundary, *J. Geophys. Res.*, *90*, 4099–4116.

Lybekk, B., A. Pedersen, S. Haaland, K. Svenes, A. N. Fazakerley, A. Masson, M. G. Taylor, and J.-G. Trotignon (2012), Solar cycle variations of the Cluster spacecraft potential and its use for electron density estimations, *J. Geophys. Res.*, *117*, A01217, doi:10.1029/2011JA016969.

McComas, D. J., P. Riley, J. T. Gosling, A. Balogh, and R. Forsyth (1998), Ulysses' rapid crossing of the polar coronal hole boundary, *J. Geophys. Res.*, *103*, 1955–1967.

Moore, T. E., and J. L. Horwitz (2007), Stellar ablation of planetary atmospheres, *Rev. Geophys.*, *45*, RG3002, doi:10.1029/2005RG000194.

Moore, T. E., et al. (1995), The Thermal Ion Dynamics Experiment and Plasma Source Instrument, *Space Sci. Rev.*, *71*, 409–458.

Moore, T. E., et al. (1997), High-altitude observations of the polar wind, *Science*, *277*, 349–351.

Nilsson, H., et al. (2008), An assessment of the role of the centrifugal acceleration mechanism in high altitude polar cap oxygen ion outflow, *Ann. Geophys.*, *26*, 145–157.

Nilsson, H., E. Engwall, A. Eriksson, P. A. Puhl-Quinn, and S. Arvelius (2010), Centrifugal acceleration in the magnetotail lobes, *Ann. Geophys.*, *28*, 569–576.

Øieroset, M., J. Raeder, T. D. Phan, S. Wing, J. P. McFadden, W. Li, M. Fujimoto, H. Rème, and A. Balogh (2005), Global cooling and densification of the plasma sheet during an extended period of purely northward IMF on October 22–24, 2003, *Geophys. Res. Lett.*, *32*, L12S07, doi:10.1029/2004GL021523.

Øieroset, M., T. D. Phan, V. Angelopoulos, J. P. Eastwood, J. McFadden, D. Larson, C. W. Carlson, K.-H. Glassmeier, M. Fujimoto, and J. Raeder (2008), THEMIS multi-spacecraft observations of magnetosheath plasma penetration deep into the dayside low-latitude magnetosphere for northward and strong B_y IMF, *Geophys. Res. Lett.*, *35*, L17S11, doi:10.1029/2008GL033661.

Paschmann, G. (1997), Observational evidence for transfer of plasma across the magnetopause, *Space Sci. Rev.*, *80*, 217–234.

Paschmann, G., et al. (1997), The electron drift instrument for Cluster, *Space Sci. Rev.*, *79*, 233–269.

Paschmann, G., et al. (2001), The electron drift instrument on Cluster: Overview of first results, *Ann. Geophys.*, *19*, 1273–1288.

Pedersen, A., F. Mozer, and G. Gustafsson (1998), Electric field measurements in a tenuous plasma with spherical double probes, in *Measurement Techniques in Space Plasmas—Fields*, edited by R. F. Pfaff, J. E. Borovsky, and D. T. Young, pp. 1–12, AGU, Washington, D. C.

Pedersen, A., P. Décréau, C. Escoubet, G. Gustafsson, H. Laakso, P. Lindqvist, B. Lybekk, A. Masson, F. Mozer, and A. Vaivads (2001), Four-point high time resolution information on electron densities by the electric field experiments (EFW) on Cluster, *Ann. Geophys.*, *19*, 1483–1489.

Pedersen, A., et al. (2008), Electron density estimations derived from spacecraft potential measurements on Cluster in tenuous plasma regions, *J. Geophys. Res.*, *113*, A07S33, doi:10.1029/2007JA012636.

Riedler, W., et al. (1997), Active spacecraft potential control, *Space Sci. Rev.*, *79*, 271–302.

Sandholt, P. E., C. J. Farrugia, S. W. H. Cowley, W. F. Denig, M. Lester, J. Moen, and B. Lybekk (1999), Capture of magnetosheath plasma by the magnetosphere during northward IMF, *Geophys. Res. Lett.*, *26*, 2833–2836.

Su, Y.-J., J. L. Horwitz, T. E. Moore, B. L. Giles, M. O. Chandler, P. D. Craven, M. Hirahara, and C. J. Pollock (1998), Polar wind survey with the Thermal Ion Dynamics Experiment/Plasma Source Instrument suite aboard Polar, *J. Geophys. Res.*, *103*, 29,305–29,338.

Svenes, K., B. Lybekk, A. Pedersen, and S. Haaland (2008), Cluster observations of magnetospheric lobe plasma densities for different solar wind conditions—A statistical study, *Ann. Geophys.*, *26*, 2845–2852.

Torkar, K., et al. (2001), Active spacecraft potential control for Cluster—Implementation and first results, *Ann. Geophys.*, *19*, 1289–1302.

Trotignon, J. G., et al. (2001), How to determine the thermal electron density and the magnetic field strength from the Cluster/Whisper observations around the Earth, *Ann. Geophys.*, *19*, 1711–1720.
Weimer, D. R., and J. H. King (2008), Improved calculations of interplanetary magnetic field phase front angles and propagation time delays, *J. Geophys. Res.*, *113*, A01105, doi:10.1029/2007JA012452.
Wilken, B., et al. (1997), RAPID—The imaging energetic particle spectrometer on Cluster, *Space Sci. Rev.*, *79*, 399–473.
Wing, S., J. R. Johnson, and M. Fujimoto (2006), Timescale for the formation of the cold-dense plasma sheet: A case study, *Geophys. Res. Lett.*, *33*, L23106, doi:10.1029/2006GL027110.
Woods, T. N., F. G. Eparvier, S. M. Bailey, P. C. Chamberlin, J. Lean, G. J. Rottman, S. C. Solomon, W. K. Tobiska, and D. L. Woodraska (2005), Solar EUV Experiment (SEE): Mission overview and first results, *J. Geophys. Res.*, *110*, A01312, doi:10.1029/2004JA010765.
Yau, A. W., and M. Andre (1997), Sources of ion outflow in the high latitude ionosphere, *Space Sci. Rev.*, *80*, 1–25.
Young, D. T., H. Balsiger, and J. Geiss (1982), Correlations of magnetospheric ion composition with geomagnetic and solar activity, *J. Geophys. Res.*, *87*, 9077–9096.

S. Haaland, Max-Planck-Institute for Solar System Research, Max-Planck-Strasse 2, D-37191 Katlenburg-Lindau, Germany. (stein.haaland@issi.unibe.ch)
B. Lybekk and A. Pedersen, Department of Physics, University of Oslo, N-0316 Oslo, Norway.
K. Svenes, Norwegian Defence Research Establishment, N-2027 Kjeller, Norway.